This article has been accepted for publication in a future issue of this journal, but has not been fully edited. Content may change prior to final publication. Citation information: DOI 10.1109/TEC.2019.2944424, IEEE Transactions on Energy Conversion

Modeling and Dynamic Performance Analysis of Brushless Doubly Fed Induction Machine Considering Iron Loss

H. R. Mosaddegh Hesar, H. Abootorabi Zarchi, and G. R. Arab Markadeh

***Abstract*— Brushless doubly fed induction machine (BDFIM) which is able to operate in both induction mode and synchronous mode, has received increasing attention of researchers, in the last three decades. It could be considered as an emerging competitor for older structures, due to the substantial features such as brushless structure and requiring a fractionally rated frequency converter. The iron loss which constitutes a significant portion of total power losses is higher in BDFIM in contrast with standard induction machine. Even though it is essential to consider the iron loss effect on dynamic behavior of BDFIM, there is still no comprehensive study in the literature. The aim of this paper is to propose a dynamic model of BFIM in general reference frame in which the iron loss is taken into account. This model which is credible for all BDFIM operation modes including synchronous one, facilitates the performance analysis of BDFIM and implementation of the various control techniques. The supplementary simulations and experiments confirm that the proposed model is an appropriate candidate for BDFIM drives. Because of the complex structure of BDFIM, determination of the iron loss isn't straightforward. In this paper, a practical approach is introduced to calculate the iron loss of BDFIM in terms of frequency variations. The experimental data derived from a D132s prototype BDFIM is then compared with the calculated data from the finite element analysis (FEA).**

***Index Terms*— Brushless doubly fed induction machine (BDFIM); iron loss resistance; reduced-order model.**

NOMENCLATURE

$\vec{V}, \vec{I}, \vec{\lambda}$	Voltage, current, flux vectors
T_e	Electromagnetic torque
P	Power
B	Flux density
R	Winding resistance
L_l	Leakage inductance
L_{pr}, L_{cr}	Coupling inductances between stator windings and rotor
p	Pole pair number
N_r	Number of rotor loops (nests)
ω_r	Synchronous rotor speed
ω	Angular speed
ω_n	Natural synchronous speed
f	Frequency
s	Slip
θ	Angular position
Subscripts	
p, c, r	Power winding (PW), control winding (CW), rotor
d, q	Rotating d-q frame axis

I. INTRODUCTION

Modelling and performance analysis of the brushless doubly fed induction machine (BDFIM) is an interesting topic which has been studied over the past few decades. The coupled-circuit dynamic model was proposed for BDFIM by *Wallace* at Oregon state university, early in the 1990s [1, 2]. This model which applies standard coupled-circuit theory to the BDFIM was used to investigate the machine performance. The derived model employs position-dependent mutual inductance matrices, which means it is not possible to solve the equations analytically for any condition except the standstill. *Li et al.* used the d-q model for the 6/2 machine of [3], to introduce an equivalent circuit representation. The suggested model is derived from equations of interacting stator coils and rotor loops by applying a mathematical transformation procedure. This model is generalized to any pole pair configuration of BDFM in [4]. Considering the BDFM as two interconnected induction machines, a steady-state equivalent circuit is developed in [5] which is valid for all modes of operation. This model has a complicated structure which makes analysis and control design of BDFIM difficult. This complexity is increased by considering the iron loss effects. To facilitate the implementation of control approaches, a simplified model excluding the iron loss has been introduced in [6]. This model is a much better approximation to represent the behavior of BDFIM compared to the core model derived by *McMahon et. al* [7]. The core model obtained by omitting the magnetizing reactances and the stator and rotor resistances is an over-simplified version of the equivalent circuit of BDFIM.

The iron loss is known as a significant factor to degrade the performance of electrical machines when they don't operate in nominal condition. Furthermore, it is a possible source which deteriorates the performance of both field-oriented control (FOC) and direct torque control (DTC). In [8, 9], the effect of the iron loss on the performance of induction motor (IM) drive has been discussed and it is shown that by neglecting the iron loss a certain amount of detuning will take place for the control schemes. The iron loss of BDFIM is higher than the conventional IM with the same capacity because of the spatial harmonic distortion of the air-gap field, non-uniform distribution of the magnetic field, and operating far from synchronous speeds of both stator fields [10]. Hence, it is required to study the BDFIM with considering the iron loss. In [11], the steady-state model of BDFIM is modified to take into account the stator and rotor iron loss. The performance of a laboratory BDFIM set-up is then evaluated by using this model. The slip-dependence of iron loss resistances have been investigated by applying energy conservation principle to derive the steady-state torque–speed relations of BDFIM in the presence of iron loss. In [12], the expressions of iron loss components created by each stator winding field are analytically derived to promote the steady-state equivalent model presented in [11]. A modified model is then developed by considering these components. The dynamic equivalent circuit of BDFIM including the iron loss has been presented in

[13]. This paper is only dealing with the stator iron loss resistance at PW side.

According to aforementioned review, there is still no comprehensive study in the literature to consider the iron loss effect on dynamic behavior of BDFIM. The main purpose of this paper is to fill this void. In this regard, the complete dynamic model of the BDFIM is derived in an arbitrary reference frame considering the iron loss, first. This model is however more complex than the ideal one. This complexity is because of the iron loss consideration as well as the existence of resistance and voltage source in the rotor loop. To overcome the complexities of the complete model, a reduced-order model is then developed tacking iron loss into account. The proposed model is formed by ignoring the contribution of direct cross-couplings between stator and rotor fields. Thus, the BDFIM model becomes similar to conventional DFIMs.

Due to the complex model of BDFIM, most of its parameters cannot be determined using the no-load and locked-rotor tests, unlike the standard IM. To find the values of equivalent circuit parameters for the BDFIM except the iron loss resistances, the identification techniques have been introduced in [14, 15] based on the recursive least square (RLS) algorithm. In this research work, the experiments are performed on a D132s prototype BDFIM whose parameters have been determined by proposed procedures in [14]. To identify the BDFIM iron loss resistances in the synchronous mode, a novel approach is presented in which the speed-dependent iron loss resistances are obtained through some effective experiments, for the first time. Detailed description of the proposed approach will be presented in the following sections. The acceptable accuracy of this method is validated by comparing the calculated iron loss resistances of BDFIM with the measured data.

This paper is organized as follows; in Section II a brief description on fundamental of BDFIM is discussed. In Section III an algorithm is introduced to calculate the iron loss resistances. In this Section, the accuracy of the presented approach is verified by FE simulation and experiments. In Section IV the reduced-order model of BDFIM including iron loss is proposed. In Section V, the simulation and the experimental results are presented. Section VI contains the concluding remarks.

II. BDFIM Modeling

A. Fundamental of BDFIM

The BDFIM is a single frame and brushless machine which has two balanced 3-phase stator windings, *i.e.* the PW and the CW. In order to avoid direct coupling, it is essential that the two windings on the stator have different numbers of poles. To reduce the electromagnetic forces on the rotor and thus to prevent the vibration, the difference between pole pairs must be greater than one [16]. There are two distinct modes of operation; the induction mode (simple induction and cascade induction) and the synchronous mode. In the simple induction mode, one of the stator windings is opened whilst the other is supplied. This situation can take place on event of converter failure, for instance. In the cascade induction mode, one of the stator windings is supplied and the other one is shorted. In this mode, the BDFIM can be considered as two induction machines with rotors connected together both electrically and mechanically, which behaves as an induction machine with $p_p + p_c$ pole pair. The most attractive mode of operation is synchronous mode. In this mode, due to the indirect coupling effect, the frequencies of the rotor currents induced by the two counter-rotating fields of the two stator windings become identical [17].

B. Principle of Operation

The resultant air-gap flux density due to the both stator windings can be expressed as follows [16]:

$$B_p(\theta,t) = B_{p\max}\cos(\omega_p t - p_p\theta + \theta_p) \quad (1)$$

$$B_c(\theta,t) = B_{c\max}\cos(\omega_c t - p_c\theta + \theta_c) \quad (2)$$

Expressing the flux densities in the rotor coordinates:

$$B_p(\theta',t) = B_{p\max}\cos((\omega_p - p_p\omega_r)t - p_p\theta' + \theta_p) \quad (3)$$

$$B_c(\theta',t) = B_{c\max}\cos((\omega_c - p_c\omega_r)t - p_c\theta' + \theta_c) \quad (4)$$

Since $\cos\theta = \cos(-\theta)$, it follows that:

$$B_c(\theta',t) = B_{c\max}\cos(-(\omega_c - p_c\omega_r)t + p_c\theta' - \theta_c) \quad (5)$$

Therefore from (3) and (5):

$$B_r(\theta',t) = B_p(\theta',t) + B_c(\theta',t) \quad (6)$$

To couple both the PW and the CW fluxes via the rotor, the frequency of currents induced in the rotor bars by two stator windings should be same. Hence, the synchronous speed of the BDFIM is given by [16]:

$$\omega_p - p_p\omega_r = -(\omega_c - p_c\omega_r) \Rightarrow \omega_r = \frac{\omega_p + \omega_c}{N_r} \quad (7)$$

Equation (7) indicates that the BDFIM rotor speed can be controlled by adjusting the CW frequency. In other words, the synchronous rotor speed is independent of the load torque unless a severe disturbance occurs. When the CW is fed by zero frequency, the natural synchronous speed will be achieved.

III. Iron Loss Calculation Algorithm

The iron loss is mainly divided into the eddy current loss and hysteresis loss. In the BDFIM, the stator tooth and yoke regions include two fundamental flux components with different frequencies while the rotor magnetic field has a single frequency. In [10], it has been shown how the BDFIM iron losses are derived including the eddy current loss and the hysteresis loss. The energetic balance of BDFIM in no-load test can be given by:

$$\begin{aligned} P_{no-load} &= P_{cu}^{PW} + P_{cu}^{CW} + P_{cu}^{r} + P_{f\&w} \\ &+ P_{iron}^{PW} + P_{iron}^{CW} + P_{iron}^{r} + P_{sll} \end{aligned} \quad (8)$$

where P_{cu}^{PW}: PW copper loss, P_{cu}^{CW}: CW copper loss, P_{cu}^{r}: rotor copper loss, $P_{f\&w}$: friction and windage loss, P_{iron}^{PW}: PW iron loss, P_{iron}^{CW}: CW iron loss, P_{iron}^{r}: rotor iron loss, and P_{sll}: stray load loss. According to (8), to separately compute the iron loss for PW and CW sides, the other losses items must be subtracted from input power $P_{no-load}$, in the first step. Due to the fact that PW is connected directly to the grid, the PW iron loss is constant [11]. Another iron loss corresponding to the CW side is slip-dependent. This component is made up of the rotor and CW iron losses. In the second step, the difference between total iron losses obtained from previous step and PW iron loss is recognized as the CW side iron loss ($P_{i,eq}$). The flowchart of iron loss calculation is shown in Fig. 1, in detail.

In order to predict the iron losses components precisely and to compare with the proposed approach, a 2D magneto-dynamic finite element (FE) model has been used. Due to the complex rotor structure, the suitable external circuit has been designed

This article has been accepted for publication in a future issue of this journal, but has not been fully edited. Content may change prior to final publication. Citation information: DOI 10.1109/TEC.2019.2944424, IEEE Transactions on Energy Conversion

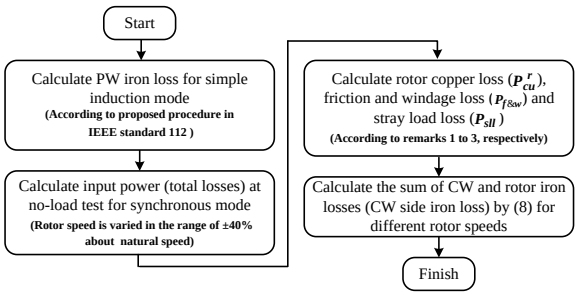

Fig. 1. Flowchart of iron loss calculation

and used. The nonlinear B-H characteristic of the magnetic steel sheet used in the rotor and stator core (M470-50A grade) is exactly defined in the finite element simulation. The required parameters for iron loss calculation are considered in accordance with Table 1. The number and quality of the generated mesh of model play a significant role in the accuracy and stability of the numerical computation. In the 2D-FE simulation due to the special geometric structure of nested loop rotor the complete machine cross-section has been used with 63998 triangular elements.

TABLE I
SPECIFICATION OF IRON CORE FOR D132S-BDFIM

Parameter	Value
Hysteresis loss coefficient	159
Eddy current loss coefficient	0.871
Lamination thickness	0.5 mm
Resistivity	420 nΩm
Mass density	7750 kg/m^3
Packing factor	0.96

Remark 1: The rotor copper loss can be calculated by $P_{cu}^r = 3R_r\left|\vec{I}_r\right|^2$. The $\vec{I}_r$ may be written as $\frac{\vec{V}_{rp}-\vec{V}_{rc}}{Z_r}$ [see Fig. 2], therefore the absolute value of rotor current is determined by applying KVL to the rotor loop:

$$\left|\vec{I}_r\right| = \sqrt{\left(\left|\vec{V}_{rp}\right|^2 - 2\left|\vec{V}_{rp}\right|\left|\vec{V}_{rp}\right|\cos\delta + \left|\vec{V}_{rc}\right|^2\right) \Big/ \left(\left(\frac{R_r}{s_p}\right)^2 + (X_{lr})^2\right)} \quad (9)$$

where δ is the phase angle between $\vec{V}_p$ and $\vec{V}_c$. By ignoring the voltage drop on the PW and the CW impedances due to the no-load operation, $\delta = \angle\vec{V}_{rp} - \angle\vec{V}_{rc}$. It is difficult to find an analytical relationship for δ, hence the value of this angle is calculated using the PW active power expression obtained in [18]. The rotor copper loss is, therefore, determined for the operational speed range of 300-700 rpm, as shown in Fig. 3. A close agreement is observed between FE simulation and results calculated by (9).

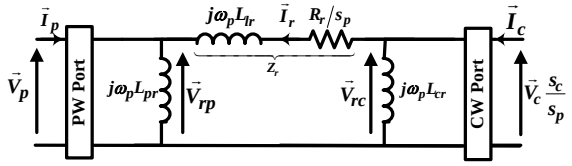

Fig. 2. Referred per-phase equivalent circuit of BDFIM [7]

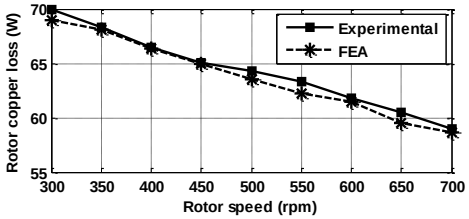

Fig. 3. Rotor copper loss versus rotor speed variations

Remark 2: To determine the friction and windage loss, the no-load input power is recorded when the PW is fed and the CW is left open. Then, the PW copper loss is subtracted from input power at each test voltage point and the resulting power curve is plotted versus square of excitation voltage. As shown in Fig. 4, the windage and friction loss for PW synchronous speed ($\omega_{PW} = 50\pi$) is approximately obtained by finding the intersection point of this curve and the power axis [19]. To measure the friction and windage loss for $10\pi \le \omega_r \le 70\pi/3$, the power related to mechanical loss can be simplistically modelled as a quadratic function of the rotor speed [20]:

$$P_{f\&w} = P_{f\&w,rated}\left(\omega_r/\omega_{r,rated}\right)^2 \quad (10)$$

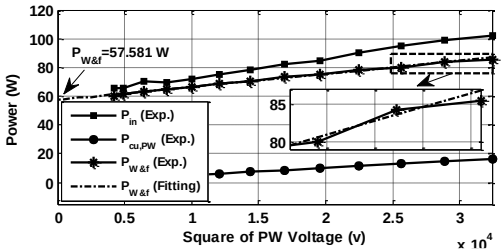

Fig. 4. No-load test results to calculate $P_{f\&w,rated}$ (simple induction mode)

Remark 3: In [10], the stray load loss of BDFIM has been calculated based on the design data and experimental parameters. A portion of the P_{sll} is owing to mechanical imperfections, hence this power loss has different values from manufacturer to manufacturer and from machine to machine. Since the purpose of this paper isn't to accurately calculate the stray load loss, the value of this loss is considered 2.2% of input power, according to the [21].

Remark 4: Since the PW is connected directly to the grid, the PW iron loss is constant. The corresponding resistance is almost 1025Ω at the rated voltage and frequency.

According to the above-mentioned points, the BDFIM iron loss resistance corresponding to the rotor and the CW is obtained. The experimental setup specifications are given in section V. To measure the CW side iron loss, the PW is fed by a 180 v (line to line voltage) and 50 Hz balanced three-phase source and the CW is controlled by using a conventional V/f algorithm to keep the magnitude of CW flux at an appropriate level. The CW side iron loss curve is illustrated in Fig. 5 over the desired operating speed interval which is derived from experimental measurements, and FE simulations. Considering

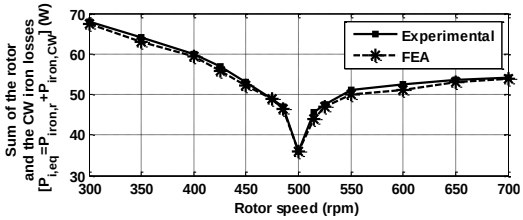

Fig. 5.Variation of CW side iron loss ($P_{i,eq}$) versus rotational speed

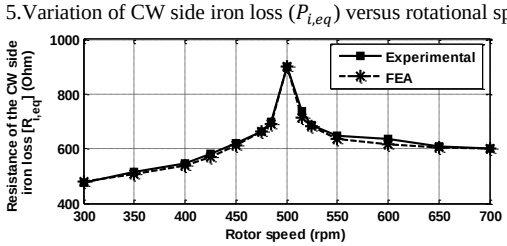

Fig. 6. Experimental and FEA results for obtaining the sum of the rotor and CW iron loss resistance ($R_{i,eq}$)

This article has been accepted for publication in a future issue of this journal, but has not been fully edited. Content may change prior to final publication. Citation information: DOI 10.1109/TEC.2019.2944424, IEEE Transactions on Energy Conversion

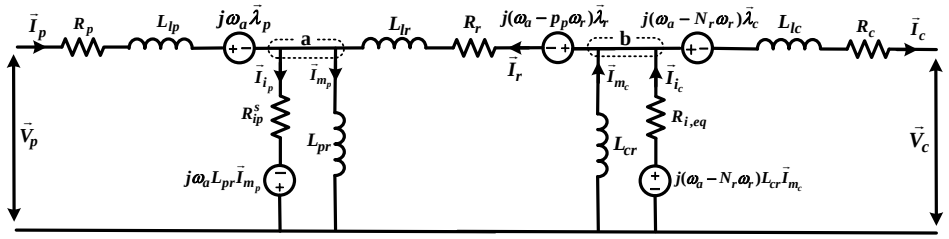

Fig. 7. Space vector equivalent circuit of BDFIM including iron loss (complete model)

$R_{i,eq} = 3V_{L-L}^2/P_{i,eq}$ and Fig. 5, the resistance of the CW side iron loss is obtained versus rotor speed varied in the range of ±40% around the natural synchronous speed. The calculated and measured results shown in Fig. 6 have a good agreement which verify acceptable accuracy of the presented analytical procedure.

IV. Reduced-Order Dynamic Model of BDFIM Including Iron Loss Model

By connecting R_{ip}^s and $R_{i,eq}$ across the magnetizing branches, the complete model of BDFIM including the iron loss is shown in Fig. 7. To derive a general model which is valid for all reference frames, two dependent voltage sources are placed series with the iron loss resistances. This model combines a well-known dynamic equivalent circuit of BDFIM excluding the iron loss with the conventional approach to model the iron loss in the space vector equivalent circuit [22]. From Fig. 7, in an arbitrary reference frame (ω_a) the expressions for the voltages and flux linkages are obtained in the form:

$$\vec{V}_p = R_p\vec{I}_p + d\vec{\lambda}_p/dt + j\omega_a\vec{\lambda}_p \quad (11)$$

$$\vec{V}_c = R_c\vec{I}_c + d\vec{\lambda}_c/dt + j(\omega_a - N_r\omega_r)\vec{\lambda}_c \quad (12)$$

$$\vec{V}_r = 0 = R_r\vec{I}_r + d\vec{\lambda}_r/dt + j(\omega_a - p_p\omega_r)\vec{\lambda}_r \quad (13)$$

$$\vec{\lambda}_p = L_{lp}\vec{I}_p + L_{pr}\vec{I}_{m_p} \quad (14)$$

$$\vec{\lambda}_c = L_{lc}\vec{I}_c + L_{cr}\vec{I}_{m_c} \quad (15)$$

$$\vec{\lambda}_r = L_{lr}\vec{I}_r + L_{pr}\vec{I}_{m_p} + L_{cr}\vec{I}_{m_c} \quad (16)$$

$$R_{ip}^s\vec{I}_{i_p} = d(L_{pr}\vec{I}_{m_p})/dt + j\omega_a L_{pr}\vec{I}_{m_p} \quad (17)$$

$$R_{i,eq}\vec{I}_{i_c} = d(L_{cr}\vec{I}_{m_c})/dt + j(\omega_a - N_r\omega_r)L_{cr}\vec{I}_{m_c} \quad (18)$$

$$T_e = 1.5\,p_p\,L_{pr}\,\mathrm{Im}\left(\vec{I}_{m_p}.\vec{I}_r^*\right) - 1.5\,p_c\,L_{cr}\,\mathrm{Im}\left(\vec{I}_{m_c}.\vec{I}_r^*\right) \quad (19)$$

In Appendix, it is shown how (19) is derived. The BDFIM consists of three torque components. The first component is the synchronous torque which exists due to the indirect coupling of the two stator windings magnetic fields. The other two components are asynchronous torques produced by direct coupling of the PW and the rotor (first induction machine), as well as the CW and the rotor (second induction machine) [23]. It should be noted that the couplings between stator and rotor fields are poorer than the indirect cross-coupling between stator fields, hence the induction machines are negligible. In other words, the resistance and the voltage source can be disregarded in the rotor loop [6]. The induction machine without presence of rotor resistance cannot produce torque, however the power conversion and the torque production will perform in BDFIM even by neglecting the rotor resistance. In [7], it has been shown by ignoring the rotor resistance, the torque expression can be written similar to a conventional synchronous machine. Due to the high spatial harmonic content of the rotor field, the rotor leakage reactance is relatively large and cannot be neglected.

In light of foregoing, by applying Δ/Y transform to the rotor reactance loop, the following expressions are obtained based on the inductances of the BDFIM complete model:

$$L_1 = \frac{L_{pr}.L_{lr}}{L_{pr}+L_{cr}+L_{lr}} \quad , \quad L_2 = \frac{L_{cr}.L_{lr}}{L_{pr}+L_{cr}+L_{lr}} \quad , \quad L_3 = \frac{L_{pr}.L_{cr}}{L_{pr}+L_{cr}+L_{lr}} \quad (20)$$

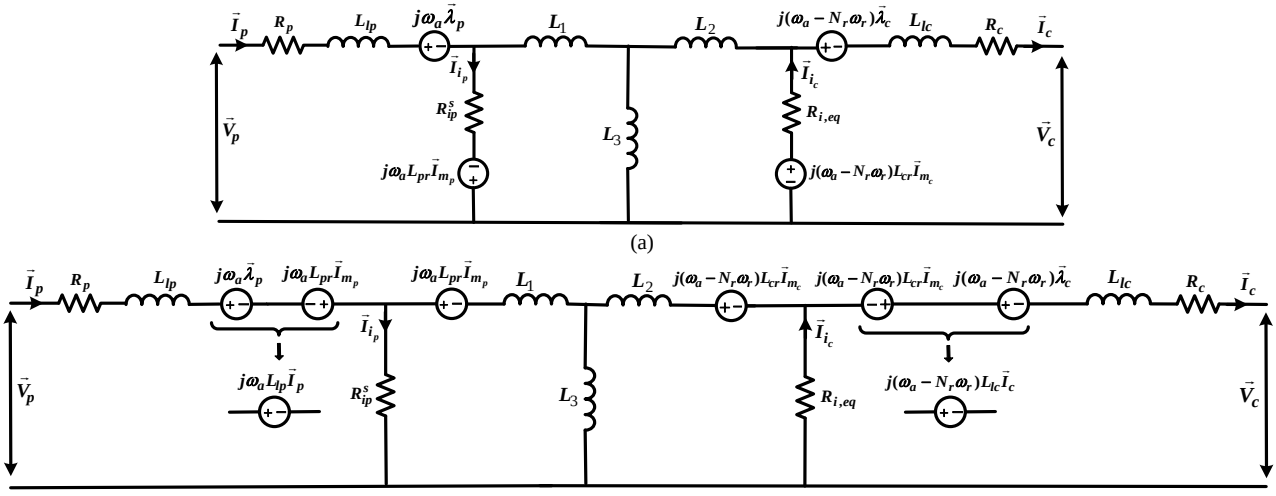

(a)

(b)

Fig.8. Process of reducing the order of BDFIM dynamic model; (a) Applying Δ→Y transform to the rotor reactance loop, (b) Shifting voltage sources to the adjacent branches

This article has been accepted for publication in a future issue of this journal, but has not been fully edited. Content may change prior to final publication. Citation information: DOI 10.1109/TEC.2019.2944424, IEEE Transactions on Energy Conversion

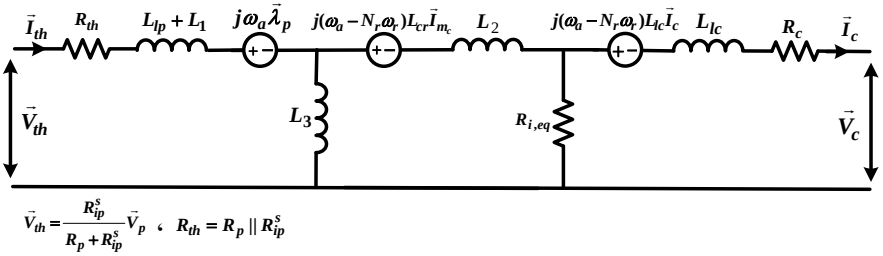

Fig. 9. Reduced-order dynamic equivalent circuit of BDFIM

Note that after substituting the *Y* model of inductances into equivalent circuit, the series voltage sources corresponding to the iron loss resistances can be shifted to the adjacent branches. To achieve the purpose, the above mentioned points are fulfilled in two steps as shown in Fig. 8.

Applying KCL in Fig. 7 for nodes "a" and "b" and after some manipulations, $\vec{I}_{m_p}$ and $\vec{I}_{m_c}$ are obtained for voltage sources in Fig. 7 as:

$$\vec{I}_{m_p}=\left(\frac{L_{lr}+L_{cr}}{L_r}\right).\left(\vec{I}_p-\vec{I}_{i_p}\right)-\frac{L_{cr}}{L_r}.\left(\vec{I}_c-\vec{I}_{i_c}\right) \quad (21)$$

$$\vec{I}_{m_c}=-\frac{L_{pr}}{L_r}.\left(\vec{I}_p-\vec{I}_{i_p}\right)+\left(\frac{L_{lr}+L_{pr}}{L_r}\right).\left(\vec{I}_c-\vec{I}_{i_c}\right) \quad (22)$$

where $L_r=L_{pr}+L_{cr}+L_{lr}$.

To develop the dynamic model for BDFIM, R^s_{ip} is placed immediately after the PW resistance. For our aim this placement is more convenient without loss of the performance accuracy, as noted in [8]. The reduced-order dynamic model for the BDFIM including the iron loss resistances is finally derived as shown in Fig. 9. Subscript "th" refers to the Thevenin's equivalent circuit seen from PW side. The voltage and flux linkage expressions for reduced-order dynamic model can now be written as:

$$\vec{V}_{th}=R_{th}\vec{I}_{th}+d\vec{\lambda}_p/dt+j\omega_a\vec{\lambda}_p \quad (23)$$

$$\vec{V}_c=R_c\vec{I}_c+d\vec{\lambda}_c/dt+j(\omega_a-N_r\omega_r)\vec{\lambda}_c \quad (24)$$

$$\vec{\lambda}_p=(L_{lp}+L_1+L_3)\vec{I}_{th}-L_3(\vec{I}_c-\vec{I}_{i_c}) \quad (25)$$

$$\vec{\lambda}_c=-L_3\vec{I}_{th}+(L_2+L_3)(\vec{I}_c-\vec{I}_{i_c})+L_{lc}\vec{I}_c \quad (26)$$

$$T_e=1.5N_r\,\mathrm{Im}\left(\vec{\lambda}_c.\vec{I}^*_c\right)-1.5N_rL_{cr}\,\mathrm{Im}\left(\vec{I}_{m_2}.\vec{I}^*_{i_c}\right) \quad (27)$$

V. Results and Discussions

The overall block diagram of the drive system is illustrated in Fig. 10.a. Tables II and III show the significant parameters of the D132s BDFIM prototype and DC generator, respectively. To couple the stator magnetic fields indirectly, the BDFIM rotor has been traditionally designed as nested-loop. There are six nests in the rotor and the natural synchronous speed is 500 rpm. This speed is considered as base value for per-unit speed. The performance of the proposed system is evaluated through a DSP-based prototype system. The experimental setup shown in Fig. 10.b consists of: a voltage source inverter with corresponding driver board, a sensor board and a TMS320F28335 signal processor board designed with Texas Instrument Co. The rotor speed is measured by a 1024 pulses incremental encoder mounted on the BDFIM shaft. The stator phase currents are measured using Hall-effect current sensors and the line-to-line voltages are detected by voltage sensors. To measure the torque, the separated excitation dc generator with an external rheostat in the armature terminal as a load is connected to the shaft of the BDFIM.

TABLE II
D132s Prototype BDFIM Parameters

Parameter	Value	Parameter	Value
PW/CW pole-pairs	2/4	R_c (Ω)	3.7171
PW rated voltage (V)	180 (at 50 Hz)	R_r (Ω)	1.1237
CW rated voltage (V)	180 (at 50 Hz)	L_{pr} (H)	0.1863
PW rated current (A)	10	L_{cr} (H)	0.0998
CW rated current (A)	4.5	L_{lp} (H)	0.0047
Rated torque (N.m)	20	L_{lc} (H)	0.0053
R_p (Ω)	1.3012	L_{lr} (H)	0.0206

TABLE III
DC Generator Specifications

Parameter	Value	Parameter	Value
Power (kW)	4.8	Rated current (A)	21
Rated voltage (V)	230	Rotor speed (rpm)	1500

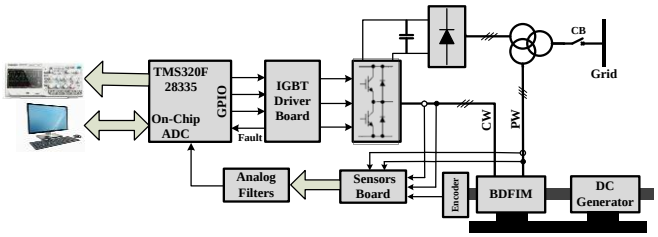

(a)

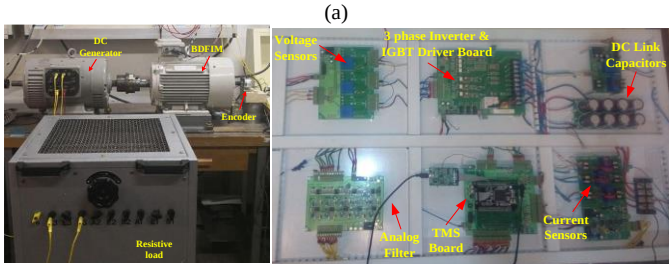

(b)

Fig. 10. Experimental setup; (a) Laboratory implementation block diagram, and (b) BDFIM drive system hardware

The dynamic performance of the proposed model is studied during the free acceleration with zero load torque. For this purpose, the nonlinear differential equations of BDFIM are simulated in MATLAB/Simulink. The rated values of torque and currents are taken as one per-unit. The BDFM is started in

This article has been accepted for publication in a future issue of this journal, but has not been fully edited. Content may change prior to final publication. Citation information: DOI 10.1109/TEC.2019.2944424, IEEE Transactions on Energy Conversion

the cascade induction mode by shorting the CW through turning on three low-side (or high-side) inverter switches. When the rotor speed approaches the natural synchronous speed, the IGBTs are controlled in the normal way to lock into the synchronous mode. Therefore, as shown in Fig. 11, the rotor speed accelerates to the natural synchronous speed. As observed, the settling time increases and the acceleration reduces when the iron loss is taken into account. Furthermore, the electromagnetic torque curves are compared in Fig. 11. The value of torque decreases with iron loss consideration. During free acceleration, the PW and the CW d-q axis currents are also obtained from complete and reduced-order models and compared with those achieved from experiments, as shown in Fig. 12

The dynamic behavior of BDFIM during step load change is illustrated in Fig. 13. The load torque is first stepped up from zero to 50% of rated torque. Then, the load torque is stepped down to zero and, as a result, the BDFIM returns to its initial operating condition.

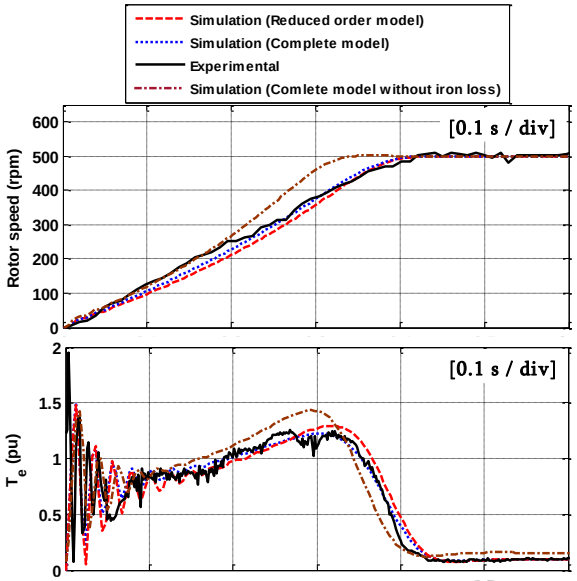

Fig. 11. Comparison of the rotor speed and the electromagnetic torque with and without iron loss (free acceleration)

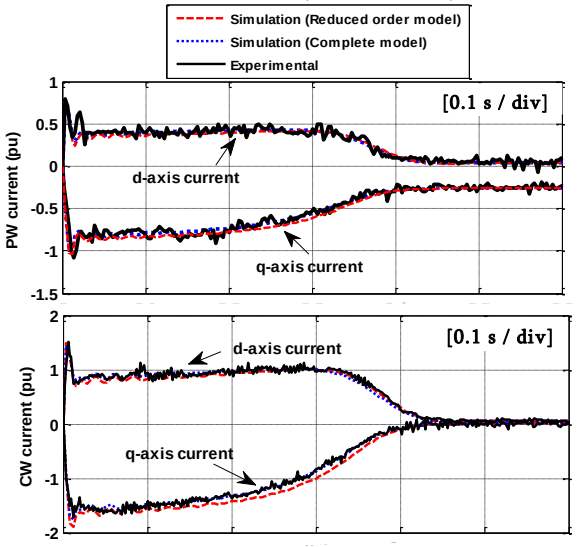

Fig. 12. Comparison of complete and reduced-order models at the cascade induction mode (free acceleration)

To more evaluate the effectiveness of the proposed model, another scenario is performed. In this case, the dynamic performance of the proposed model is investigated by applying a three-phase voltage fault at the BDFIM terminal. In this regard, the fault occurs at $t = 2$ s with opening CB. After two seconds the CB is reclosed and along with the fault clearance the terminal voltage is reapplied. With the BDFIM stator currents equal to zero, the electromagnetic torque is obviously zero; therefore the load torque decelerates the BDFIM rotor speed. The acceptable accuracy of the reduced-order model during the three-phase fault is shown in Fig. 14. A little disagreement is observed between the simulation and experimental results. Any difference between them is related to stray load loss, mechanical loss, magnetic saturation effect that is not taken into account in the BDFIM modeling, inaccuracies

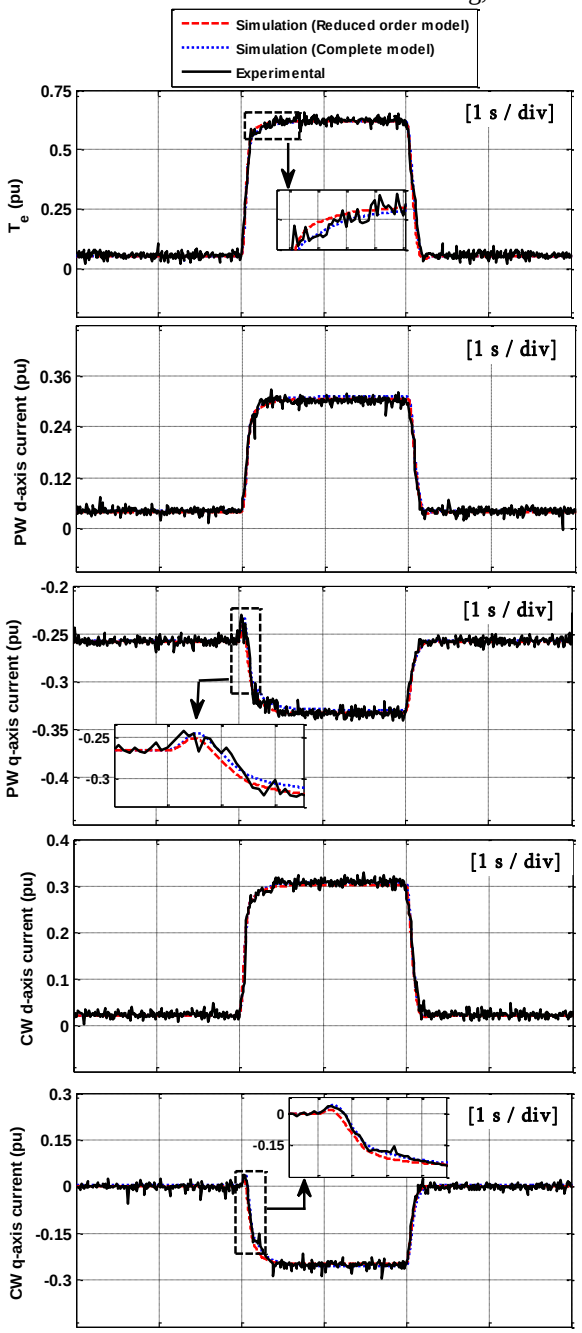

Fig. 13. Dynamic performance of BDFIM during step changes in load torque

This article has been accepted for publication in a future issue of this journal, but has not been fully edited. Content may change prior to final publication. Citation information: DOI 10.1109/TEC.2019.2944424, IEEE Transactions on Energy Conversion

that exist in the iron loss calculation, inaccurate IGBT models employed in the extraction of simulation results, inverter power switches dead times, and so on. As a result, the BDFIM can be modelled similar to the DFIM including the iron loss.

To compare the proposed model with other ones introduced in the literature, Table IV summarizes the most significant features of them. It should be noted that it is better to study the proposed BDFIM model for different operation conditions and for different machines. However the BDFIM is an emerging machine which is still at the prototyping and a few BDFIM prototypes have been fabricated only for laboratory applications. It means that the BDFIM has never been commercialized [24] and there are still challenges so as to reach the BDFIM to the commercial maturity.

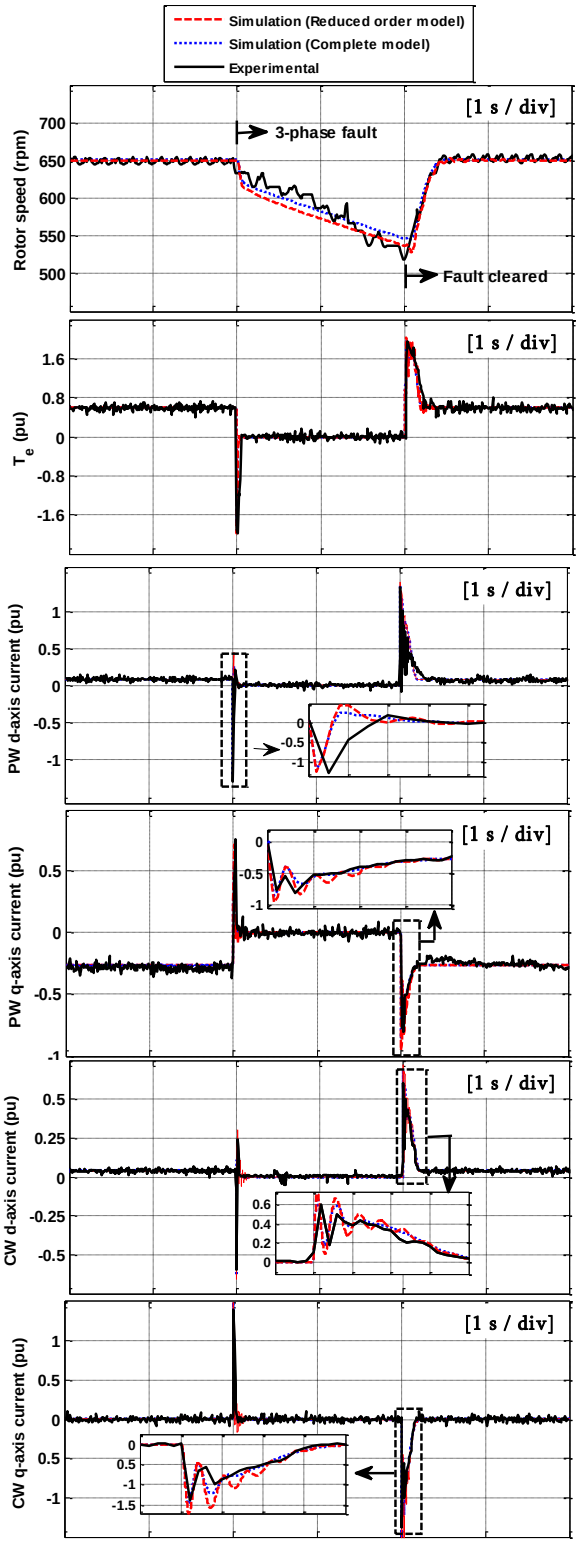

Fig. 14. Dynamic performance of BDFIM during three-phase fault

TABLE IV
COMPARISON OF BDFIM MODELS PROPOSED IN THE LITERATURE

Ref.	Rated torque	Has been iron loss considered?	Dynamic or steady-state modelling?
[1]	36 N.m	No	Dynamic
[3]	Unspecified	No	Dynamic
[5]	143 N.m	No	Steady-state
[6]	50 N.m	No	Dynamic/steady-state
[11]	27 N.m	Yes	Steady-state
Proposed model	20 N.m	Yes	Dynamic

VI. Conclusion

In this paper, a novel procedure was proposed to identify the iron losses of BDFIM and the related equivalent resistances were achieved experimentally through these data. Even though the PW side resistance is constant, the resistance corresponding to the sum of the rotor and CW iron losses is slip-dependent. The acceptable accuracy of the presented approach was verified by comparing the results obtained from FEA with the measured data. A new model was then introduced for the BDFIM which was taken iron loss effect into account. The reduced-order dynamic model not only doesn't have the complicated structure of the BDFIM model excluding the iron loss but also can correctly show the behavior of machine. The simulation and experimental results proved our claim during the free acceleration, the step changes in load torque, and the three-phase fault. As a result, this model can be considered as an attractive suggestion to study the BDFIM performance for various control strategies.

Appendix

In this Section, the detailed procedures are presented for deriving the torque equation (19). Substituting (11) and (12) into the space vector expression for active power, the total three-phase active input power can be written as follows:

$$\begin{aligned} P_{3\phi} &= \frac{3}{2}\Re\left\{\vec{V}_p\,\vec{I}_p^{\,*}+\vec{V}_c\,\vec{I}_c^{\,*}\right\} \\ &= \frac{3}{2}\Re\left\{ R_p\left|\vec{I}_p^{\,2}\right|+L_{pr}\frac{d\vec{I}_{m_p}}{dt}\vec{I}_p^{\,*}+L_{lp}\frac{d\vec{I}_p}{dt}\vec{I}_p^{\,*}+j\omega_a\,\vec{\lambda}_p\,\vec{I}_p^{\,*}\right. \\ &\left. +R_c\left|\vec{I}_c^{\,2}\right|+L_{cr}\frac{d\vec{I}_{m_c}}{dt}\vec{I}_c^{\,*}+L_{lc}\frac{d\vec{I}_c}{dt}\vec{I}_c^{\,*}+j(\omega_a-N_r\,\omega_r)\,\vec{\lambda}_c\,\vec{I}_c^{\,*}\right\} \end{aligned} \quad \text{(A-1)}$$

Using (17) and (18) and applying KCL to the nodes "a" and "b" [see Fig. 7], we have:

$$R_{ip}^{s}\left|\vec{I}_{i_p}^{\,2}\right| = L_{pr}\frac{d\vec{I}_{m_p}}{dt}\left(\vec{I}_p^{\,*}+\vec{I}_r^{\,*}-\vec{I}_{m_p}^{\,*}\right)+j\omega_a\,L_{pr}\,\vec{I}_{m_p}\,\vec{I}_{i_p}^{\,*} \quad \text{(A-2)}$$

$$R_{i,eq}\left|\vec{I}_{i_c}^{\,2}\right| = L_{cr}\frac{d\vec{I}_{m_c}}{dt}\left(\vec{I}_c^{\,*}+\vec{I}_r^{\,*}-\vec{I}_{m_c}^{\,*}\right)+j(\omega_a-N_r\,\omega_r)\,L_{cr}\,\vec{I}_{m_c}\,\vec{I}_{i_c}^{\,*} \quad \text{(A-3)}$$

Applying KVL to the rotor loop in Fig. 7, we can write:

$$L_{pr}\frac{d\vec{I}_{m_p}}{dt}+L_{cr}\frac{d\vec{I}_{m_c}}{dt}=-R_r\,\vec{I}_r-L_{lr}\frac{d\vec{I}_r}{dt}-j(\omega_a-p_p\,\omega_r)\,\vec{\lambda}_r \tag{A-4}$$

Substituting (A-2) to (A-4) into (A-1) and after some manipulations we can write the input power expression as:

$$\begin{aligned}P_{3\phi}=\frac{3}{2}\Re\Big\{&R_p\left|\vec{I}_p\right|^2+R_c\left|\vec{I}_c\right|^2+R_r\left|\vec{I}_r\right|^2+R_{ip}^s\left|\vec{I}_{i_p}\right|^2+R_{i,eq}\left|\vec{I}_{i_c}\right|^2\\&+L_{pr}\frac{d\vec{I}_{m_p}}{dt}\vec{I}_{m_p}^*-j\omega_a\,L_{pr}\,\vec{I}_{m_p}\vec{I}_{i_p}^*\\&+L_{cr}\frac{d\vec{I}_{m_c}}{dt}\vec{I}_{m_c}^*-j(\omega_a-N_r\,\omega_r)L_{cr}\,\vec{I}_{m_c}\vec{I}_{i_c}^*\\&+L_{lp}\frac{d\vec{I}_p}{dt}\vec{I}_p^*+j\omega_a\,\vec{\lambda}_p\,\vec{I}_p^*\\&+L_{lc}\frac{d\vec{I}_c}{dt}\vec{I}_c^*+j(\omega_a-N_r\,\omega_r)\,\vec{\lambda}_c\,\vec{I}_c^*\\&+L_{lr}\frac{d\vec{I}_r}{dt}\vec{I}_r^*+j(\omega_a-p_p\,\omega_r)\,\vec{\lambda}_r\,\vec{I}_r^*\Big\}\end{aligned} \tag{A-5}$$

This expression can now be broken down into its individual components as follows:

Copper and iron losses

$$=\frac{3}{2}\left(R_p\left|\vec{I}_p\right|^2+R_c\left|\vec{I}_c\right|^2+R_r\left|\vec{I}_r\right|^2+R_{ip}^s\left|\vec{I}_{i_p}\right|^2+R_{i,eq}\left|\vec{I}_{i_c}\right|^2\right)$$

Change in field energy

$$=\frac{3}{2}\Re\left\{L_{pr}\frac{d\vec{I}_{m_p}}{dt}\vec{I}_{m_p}^*+L_{cr}\frac{d\vec{I}_{m_c}}{dt}\vec{I}_{m_c}^*+L_{lp}\frac{d\vec{I}_p}{dt}\vec{I}_p^*+L_{lc}\frac{d\vec{I}_c}{dt}\vec{I}_c^*+L_{lr}\frac{d\vec{I}_r}{dt}\vec{I}_r^*\right\}$$

Rotational power

$$=\frac{3}{2}\Re\left\{-jp_p\,\omega_r\vec{\lambda}_r\,\vec{I}_r^*-jN_r\,\omega_r\vec{\lambda}_c\,\vec{I}_c^*+jN_r\,\omega_r\,L_{cr}\,\vec{I}_{m_c}\vec{I}_{i_c}^*\right\}$$

Therefore:

$$T_e=\frac{P_{rot}}{\omega_r}=\frac{3}{2}\,p_p\,L_{pr}\,\mathrm{Im}\left(\vec{I}_r^*.\vec{I}_{m_p}\right)-\frac{3}{2}\,p_c\,L_{cr}\,\mathrm{Im}\left(\vec{I}_r^*.\vec{I}_{m_c}\right) \tag{A-6}$$

REFERENCES

[1] A. K. Wallace, R. Spee, and H. K. Lauw, "Dynamic Modelling of Brushless Doubly-Fed Machines", *Conference Record of the IEEE Industry Applications Society Annual Meeting*, San Diego, USA, October 1989.

[2] R. Spee, A. K. Wallace, and H. K. Lauw, "Performance Simulation of Brushless Doubly-Fed Adjustable Speed Drives", *Conference Record of the IEEE Industry Applications Society Annual Meeting*, San Diego, USA, October 1989.

[3] R. Li, A. K. Wallace, R. Spee, and Y. Wang, "Two-axis Model Development of Cage-Rotor Brushless Doubly-Fed Machines", *IEEE Transactions on Energy Conversion*, vol. 6, no. 3, pp. 453-460, September 1991.

[4] M. S. Boger, A. K. Wallace, R. Spee, and R. Li, "General Pole Number Model of the Brushless Doubly-Fed Machine", *IEEE Transactions on Industry Applications*, vol. 31, no. 5, pp. 1022-1028, September/October 1995.

[5] P. C. Raberts, "*A Study of Brushless Doubly-Fed (Induction) Machines; Contributions in Machine Analysis, Design and Control*", PhD Thesis, University of Cambridge, September 2004.

[6] S. Tohidi, "Analysis and Simplified Modelling of Brushless Doubly-Fed Induction Machine in Synchronous Mode of Operation*", IET Electric Power Applications*, vol. 10, no. 2, pp. 110-116, February 2016.

[7] R. A. McMahon, P. C. Roberts, X. Wang, and P. J. Tavner, "Performance of BDFM as generator and motor", *IEE Electric Power Applications*, vol. 153, no. 2, pp. 289-299, March 2006.

[8] E. Levi, M. Sokola, A. Boglietti, and M. Pastorelli, "Iron Loss in Rotor-Flux-Oriented Induction Mschines: Identification, Assesment of Detuning, and Compensation", *IEEE Transactions on Power Electronics*, vol. 11, no. 5, pp. 698-709, September 1996.

[9] E. Levi, and T. Pham-Dinh, "DTC of Induction Machines Considering the Iron Loss", *Electric Power Components and Systems,* vol. 30, no. 6, pp. 557-579, 2002.

[10] H. Gorginpour, H. Oraee, and E. Abdi, "Calculation of Core and Stray Load Losses in Brushless Doubly-Fed Induction Generators", *IEEE Transactions on Industrial Electronics*, vol. 61, no. 7, pp. 3167 – 3177, July 2014.

[11] M. N. Hashemnia, F. Tahami, and E. Oyarbide, "Investigation of Core Loss Effect on Steady-State Characteristics of Inverter Fed Brushless Doubly Fed Machines", *IEEE Transactions on Energy Conversion*, vol. 29, no. 1, pp. 57-64, March 2014.

[12] M. Yousefian, H. Abootorabi Zarchi, and H. Gorginpour, "Modified Steady-State Modelling of Brushless Doubly-Fed Induction Generator Taking Core Loss Components into Account", *IEE Electric Power Applications*, 10.1049/iet-epa.2019.0133.

[13] M. N. Hashemnia, and F. Tahami, "Dynamic Modeling and Simulation of Brushless Doubly Fed Induction Machine in Consideration of Core Loss", *38th Annual Conference on IEEE Industrial Electronics Society (IECON 2012)*, Montreal, Canada, October 2012.

[14] P. C. Roberts, R. A. McMahon, P. J. Tavner, J. M. Maciejowski, and T. J. Flack, "Equivalent Circuit for the Brushless Doubly Fed Machine (BDFM) Including Parameter Estimation and Experimental verification", *IEE Electric Power Applications*, vol. 152, no. 4, pp. 933-942, July 2005.

[15] H. Djadi, K. Yazid, and M. Menaa, "Parameters Identification of a Brushless Doubly Fed Induction Machine using Pseudo-Random Binary Signal Excitation Signal for Recursive Least Squares Method", *IET Electric Power Applications*, vol. 11, no. 9, pp. 1585-1595, November 2017.

[16] WiIliamson, A. C. Ferreira, and A. K. Wallace, "Generalised Theory of the Brushless Doubly-Fed Machine. Part I: Analysis", *IEE Electric Power Applications*, vol. 144, no. 2, pp. 111-122, March 1997.

[17] R. Li, A. K. Wallace, and R. Spee, "Dynamic Simulation of Brushless Doubly-Fed Machines", *IEEE Transactions on Energy Conversion*, vol. 6, no. 3, pp. 445-452, September 1991.

[18] S. Tohidi, M.R. Zolghadri, H. Oraee, P. Tavner, E. Abdi, and T. Logan, "Performance of the Brushless Doubly-Fed Machine under Normal and Fault Conditions", *IET Electric Power Applications*, vol. 6, no. 9, pp. 621-627, November 2012.

[19] *Test Procedure for Poly-phase Induction Motors and Generators*, IEEE Standard 112 (Revision of IEEE Std 112-2004), 2017.

[20] D. Basic, J. G. Zhu, and G. Boardman, "Modeling and Steady-State Performanc Analysis of a Brushless Doubly Fed Twin Stator Induction Generator", *Australasian Power Engineering Conference (AUPEC)*, pp. 1-6, 2002.

[21] *Method for Determining Losses and Efficiency of Three-Phase Cage Induction Motors*, IEC 61972, 2002.

[22] E. Levi, "Impact of Iron Loss on Behavior of Vector Controlled Induction Machines", *IEEE Transactions on Industry Applications*, vol. 31, no. 6, pp. 1287-1296, November/December 1995.

[23] I. Sarasola, J. Poza, M. A. Rodriguez, and G. Abad, "Direct Torque ontrol Design and Experimental Evaluation for the Brushless Doubly Fed Machine", *Energy Conversion and Management*, vol. 52, no. 2, pp. 1226-1234, February 2011.

[24] T. D. Strous, H. Polinder and J. A. Ferreira, "Brushless Doubly-Fed Induction Machines for Wind Turbines: Developments and Research Challenges", *IET Electric Power Applications*, vol. 11, no. 6, pp. 991-1000, July 2017.

This article has been accepted for publication in a future issue of this journal, but has not been fully edited. Content may change prior to final publication. Citation information: DOI 10.1109/TEC.2019.2944424, IEEE Transactions on Energy Conversion

Hamidreza Mosaddegh Hesar received the B.Sc. and M.Sc. degrees from Ferdowsi University of Mashhad, Iran, in 2011 and 2014, respectively, all in electrical engineering. He is currently pursuing the Ph.D. degree at Ferdowsi University of Mashhad, Iran.

His current interests and activities include control of high-performance drives, nonlinear control, and modeling of electrical machines.

Hossein Abootorabi Zarchi received the M.S. and Ph.D. degrees from the Isfahan University of Technology, Isfahan, Iran, in 2004 and 2010, respectively. He was a Visiting Ph.D. Student with the Control and Automation Group, Denmark Technical University, Denmark, from May 2009 to February 2010. He is currently an Assistant Professor in the Department of Electrical Engineering, Ferdowsi University of Mashhad, Mashhad, Iran.

His research interests include electrical machines, applied nonlinear control in electrical drives, and renewable energies.

Gholamreza Arab Markadeh received the B.Sc., M.Sc., and Ph.D. degrees in Electrical Engineering from Isfahan University of Technology, Iran, in 1996, 1998, and 2005, respectively. He is currently an Associate Professor in the Faculty of Engineering, Shahrekord University. His fields of research include nonlinear control, power electronics, and variable-speed drives. He is the Editor-in-chief of Journal of Dam and Hydroelectric Powerplant. Dr. Arab Markadeh was the recipient of the IEEE Industrial Electronics Society IECON'04 best paper presentation award in 2004.